EFFECT OF HIGH-ORDER MODES ON TUNNELING CHARACTERISTICS

H.-Y. Yao and T.-H. Chang

Department of Physics
National Tsing Hua University
101, Section 2, Kuang Fu Road, Hsinchu, Taiwan

Abstract—Most tunneling effects are investigated using a one-dimensional model, but such an approach fails to explain the phenomena of the propagation of wave in a system with geometric discontinuities. This work studies the tunneling characteristics in a waveguide system that consists of a middle section with a distinct cutoff frequency, which is controlled by the cross-sectional geometry. Unlike in the one-dimensional case, in which only the fundamental mode is considered, in a virtually three-dimensional system, multiple modes have to be taken into consideration. High-order modes (HOMs) modify the amplitude and the phase of the fundamental mode (TE_{10}), thus subsequently affecting the transmission and group delay of a wave. The effect of the high-order evanescent modes is calculated, and the results are compared with the simulated ones using a full-wave solver. Both oversized and undersized waveguides reveal the necessity of considering the HOMs. The underlying physics is manifested using a multiple-reflection model. This study indicates that the high-order evanescent modes are essential to the explanation of the phenomena in a tunneling system with geometrical discontinuities.

1. INTRODUCTION

How long a particle takes to tunnel through a classical forbidden zone is still a controversial issue among physicists and has practical importance to applications [1–3]. Many astonishing phenomena that are related to the tunneling time are still under researching, such as the superluminal effect [4, 5] and Hartman effect [6, 7]. Such phenomena are observed in numerous systems, such as steep anomalous

---

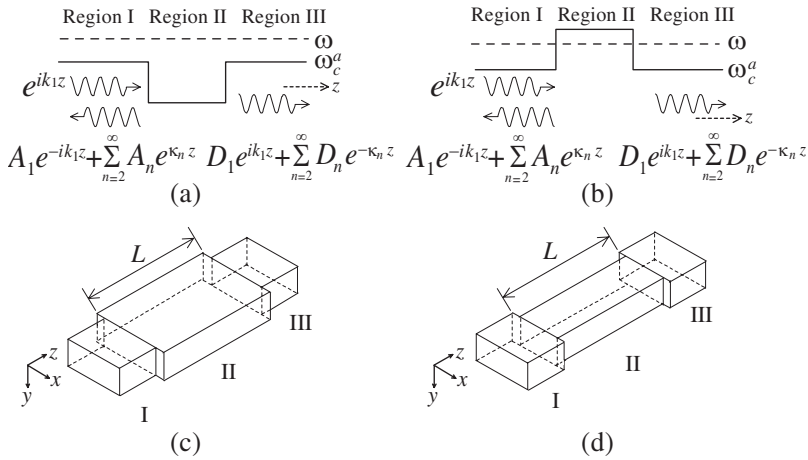Corresponding author: T.-H. Chang (thschang@phys.nthu.edu.tw).

dispersion in optical gain/absorption mediums [8–10], birefringent crystal systems [11], photonic systems [12, 13], electronic circuits [3], and waveguide systems [14–22]. Of these, the waveguide system shares many similar characteristics with its counterpart in quantum mechanics. A waveguide system is ideal to exploring the intriguing physics of the tunneling effect. Actually, in a one-dimensional waveguide system [14, 15], the theoretical model is simple in mathematics, but it cannot be applied to three-dimensional waveguide systems. When a wave passes through a geometrically discontinuous surface, however, it will excite multiple modes to satisfy the boundary conditions. Numerous previous investigations have pointed out the difficulties and the challenges of modal analysis [14, 15, 20, 21, 23, 24], but none has yet studied it systematically.

This study provides a solution to and physical interpretations of this long-standing but important problem. First, consider the following one-dimensional time-independent Schrödinger and Helmholtz equations:

$$\left[\frac{\partial^2}{\partial z^2} - \frac{2m}{\hbar^2}V(z) + \frac{2m}{\hbar^2}E\right]\varphi(z) = 0 \qquad (1a)$$

$$\left[\frac{\partial^2}{\partial z^2} - \frac{\varepsilon_r}{c^2}\omega_c^2(z) + \frac{\varepsilon_r}{c^2}\omega^2\right]B_z(z) = 0 \qquad (1b)$$

where φ, V, and E are the wave function, potential energy, and free energy of the particle; B_z, ω_c and ω are the wave component, the cutoff frequency, and the frequency of a transverse electric (TE) wave; m, $\hbar$, ε_r, and c are the mass of the particle, Plank constant, relative permittivity, and the speed of light in vacuum. The relative permeability is assumed to be unity ($\mu_r = 1$). The one-dimensional quantum system (1a) and the one-dimensional waveguide system (1b) exhibit similar characteristics. However, a waveguide system with geometrical discontinuities is a three-dimensional system. High-order evanescent modes should be considered. Fig. 1(a) and Fig. 1(b) schematically depict the passing of a wave through a potential well and a barrier, respectively. High-order modes, each with sub-index n (starting from 2 to ∞), are shown. The cutoff frequency can be changed by either alerting the cross-sectional geometry of the waveguide or inserting a dielectric material inside the waveguide. The former is achieved by using an oversized waveguide (Fig. 1(c), analogous to a potential well) or an undersized waveguide (Fig. 1(d), analogous to a potential barrier). The latter method can be made by assuming a suitable dielectric material without changing the geometry of the waveguide. Notably, a material with required dielectric properties may be difficult to find in nature.

Figure 1. Schematic diagrams of the tunneling effect and the corresponding waveguide structures: (a) a potential well, (b) a potential barrier, (c) an oversized waveguide which models a potential well, and (d) an undersized waveguide which models a potential barrier. The corresponding coordinate system is shown in Fig. 1(c) and Fig. 1(d).

All of the waveguide modes, including the propagating mode and high-order evanescent modes shown in Fig. 1(a) and Fig. 1(b), have to satisfy the boundary conditions. The effect of higher-order evanescent modes must be taken into consideration unlike in one-dimensional systems, because the excitation of these high-order evanescent modes will affect the transmission and group delay of a wave.
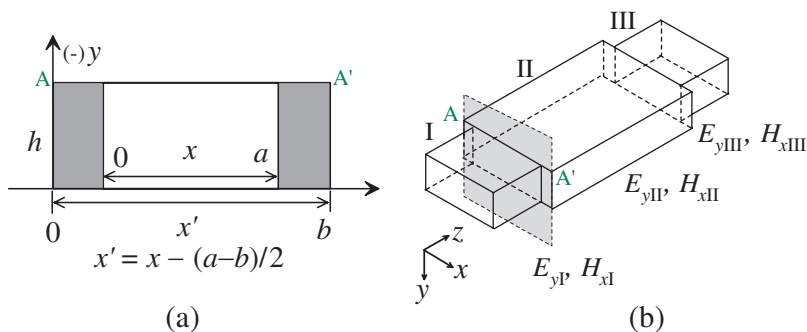
This work introduces a general microwave technique, modal analysis, to analyze the waveguide systems. Three-dimensional boundary conditions and electromagnetic field components are employed. The transmission of the fundamental mode is analogous to the tunneling probability in quantum mechanics. The group delay of the electromagnetic wave resembles the tunneling time of a matter wave in quantum mechanics. Intensive numerical calculations are conducted. The results are compared with those obtained using a full-wave electromagnetic solver.

2. MODAL ANALYSIS FOR SYMMETRIC *H*-PLANE DISCONTINUITIES

When a wave with a specific mode hits a discontinuity, it excites extra modes in addition to the original one. The incident mode, reflected modes, and transmitted modes have to jointly satisfy the boundary conditions at the discontinuity. This approach is called modal analysis, which is usually employed in microwave engineering [25–27]. In the following, a structure consisting of three rectangular waveguides with an oversized waveguide in the middle, displayed in Fig. 1(c), is analyzed. This system is analogous to a quantum potential well (Fig. 1(a)).

Figure 2(a) shows the cross-sectional view of the discontinuity. The input section (region I) and output section (region III) are standard WR-284 waveguides. The height is 34.04 mm ($h = 1.34$ inches), and the width is 72.14 mm ($a = 2.84$ inches). Typically, the cutoff frequency of WR-284 waveguide is 2.079 GHz. The oversized middle section (region II) has the same height with the waveguides in regions I and III, but the width changes to 83.33 mm ($b = 3.28$ inches) with the cutoff frequency of 1.8 GHz. Such configuration is called symmetric *H*-plane discontinuities. Moreover, the following approach can be applied to a discontinuity with arbitrary shape.

The incident mode is the fundamental TE_{10} mode. All of the high-order modes are evanescent in the range of operating frequencies.

Figure 2. (a) Cross-sectional view of the interface of the waveguide discontinuity. To simplify the notations, there are two different horizontal axes. (b) Schematic diagram of the boundary conditions where the *y*-component of the electric field and the *x*-component of the magnetic field are continuous at the interfaces.

The electric fields in regions I and III are,

Region I: $E_{yI} = \sin\left(\dfrac{\pi x}{a}\right)e^{ik_1 z} + A_1\sin\left(\dfrac{\pi x}{a}\right)e^{-ik_1 z} + \sum\limits_{n=2}^{\infty}A_n\sin\left(\dfrac{n\pi x}{a}\right)e^{\kappa_n z}$

Region III: $E_{yIII} = D_1\sin\left(\dfrac{\pi x}{a}\right)e^{ik_1 z} + \sum\limits_{n=2}^{\infty}D_n\sin\left(\dfrac{n\pi x}{a}\right)e^{-\kappa_n z}$
$$(2)$$

where $k_1 = \sqrt{(\omega^2 - \omega_{c,1}^2)}\Big/c$, $\kappa_n = \sqrt{(\omega_{c,n}^2 - \omega^2)}\Big/c$, and $\omega_{c,n}$ are the propagation constant of fundamental TE_{10} mode, the attenuation constant of nth higher-order evanescent mode, and the cutoff frequency of the nth mode, respectively. A_n and D_n are the reflection coefficient and transmission coefficient of the nth mode.

Unlike in quantum mechanics, in which the boundary conditions require that the wave function and its first derivative are continuous, in electrodynamics, the electric and magnetic fields must be continuous at the boundary.

Appendix A presents the detailed arithmetic including the complete three-dimensional boundary conditions and modal analysis. Proper manipulations and considerations of the first N modes yield,

$$P_m = \sum_{n=1}^{N} Q_{mn}D_n \qquad (3)$$

where P_m and Q_{mn} are given in the Appendix A.

Equation (3) is a matrix format which is adopted to solve D_n. From D_n, the transmission amplitude and the total phase change of the nth mode can be calculated. The aforementioned equations are developed for a potential well (Fig. 1(a) and Fig. 1(c)), while those for a potential barrier (Fig. 1(b) and Fig. 1(d)) can be obtained similarly.

3. TRANSMISSION AND GROUP DELAY WITH MODAL CORRECTION

To meet the boundary conditions of a discontinuity, extra modes are generated in addition to the original incident mode. The high-order modes function as an effective reactance, which changes the electromagnetic field energy stored within the system [26]. The extra energy stored in, or exchanged between, the electric fields and magnetic fields mainly alters the amplitude and the phase of the operating (propagating) mode. This phase change of the propagating mode affects the interference conditions leading to an offset in the resonant transmission and a variation in the group delay. The mechanism of

phase control by the excitation of evanescent modes will be elucidated in Section 4. In the following, the fundamental characteristics of the tunneling phenomena, i.e., the transmission and group delay in frequency domain are discussed.

The transmission T is defined as the transmitted power divided by the input power of the fundamental mode. Since the characteristic impedances of the input and output sections are identical, the transmission of the TE_{10} mode is simply defined as $T \equiv D_1^* \cdot D_1$. According to the stationary phase approximation, the group delay is correlated to the phase ϕ of the transmission coefficient, $D_1 = |D_1|e^{i\phi}$ and is generally defined [14, 15, 19, 22, 28] as,
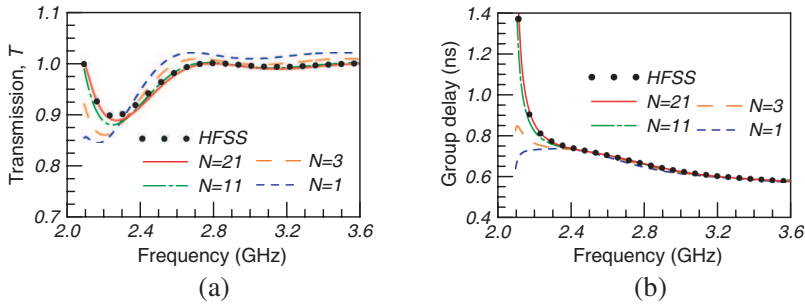
$$\tau_g = \frac{d\phi}{d\omega} \qquad (4)$$

Group delay is associated with the time lag of a wave packet passing through an obstacle. Therefore, group delay describes the time difference between the time when the peak of the wave packet enters the obstacle and the time when the peak leaves this section. Normally, group delay is positive and greater than the limit imposed by the special relativity (which is the length of the obstacle divided by the speed of light in vacuum (c)). Notably, (4) is obtained from a frequency domain result. The transmission and group delay for an oversized waveguide and an undersized waveguide are examined in Sections 3.1 and 3.2.

3.1. Oversized Waveguide: Analogy to Potential Well

A middle section of an oversized waveguide (Fig. 1(c)) in electromagnetism is analogous to a potential well shown in Fig. 1(a). Fig. 3(a) plots the transmission for $L = 15$ cm. The cutoff frequency of the TE_{10} mode for the oversized waveguide is 1.8 GHz, while those for the input and output sections (WR-284) are the same, 2.079 GHz. Modal analysis suggests that the existence of the high-order modes must be considered in the geometrically discontinuous system. $N = 1$ means that only one mode is considered; $N = 3$ means that three modes are considered and so on. As the number of considered modes increases, the results become more accurate, but too many modes may contribute more numerical errors. When 21 modes are considered, the results agree very well with the simulated ones obtained by HFSS (High Frequency Structure Simulator, Ansoft).

Figure 3(a) shows, as expected, that the modal correction is vital for the low-frequency region. In this waveguide system, the characteristic impedance changes dramatically, and the total phase difference of transmitted wave varies rapidly when the operating

Figure 3. (a) Transmission and (b) group delay as functions of frequency for the potential well with geometry shown in Fig. 1(c). In this case, L equals to 15 cm and the modal effects are displayed.
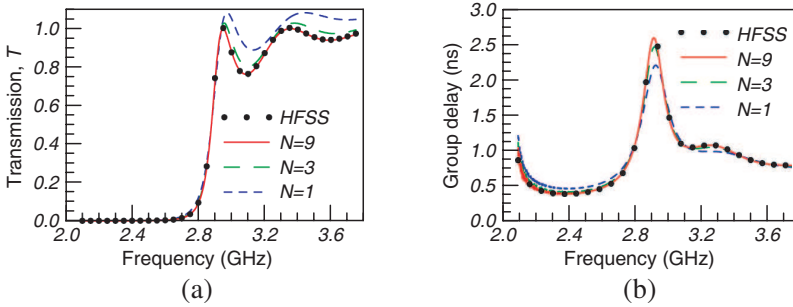
frequency is close to the cutoff, thus significantly affecting the transmission behavior. This explains why modal effect is important for transmission in low-frequency region. Even though the calculated results converge slowly as the number of modes increase, it does remedy the behavior of the wave in the near-cutoff region.

On the other hand, Fig. 3(b) shows the group delays for the system which is identical to that in Fig. 3(a). The group delay is calculated using (4). In the low-frequency region, the total phase change of the transmitted wave is sensitive to the effect of the high-order evanescent modes. Consequently, the excitation of high-order modes alters the total phase change and interference conditions. The change of the interference conditions leads to the large variation of group delay. Therefore, the group delay is corrected when the modal analysis is employed in the low-frequency region.

3.2. Undersized Waveguide: Analogy to Potential Barrier

Figure 4(a) shows the transmission response of the undersized waveguide for $L = 15$ cm. The cutoff frequency of the TE_{10} mode for the undersized waveguide is 2.8 GHz, as shown in Fig. 1(b) and Fig. 1(d). Other parameters are exactly the same as those in the oversized case. When the input wave has frequency less than 2.8 GHz, the fundamental mode is also evanescent in the middle section.

Figure 4(b) displays the group delay for the undersized waveguide. The calculated results converge very fast as the number of modes, N, increases. When $N = 9$, the calculated results (solid lines) agree well with the simulated ones (solid dots). The group delay should be generally greater than the lowest limit (L/c), but a superluminal zone exists in the frequency range from 2.3 GHz to 2.7 GHz as shown in Fig. 4(b). The group delay is independent of the frequency and the

Figure 4. (a) Transmission and (b) group delay verse the frequency for the potential barrier case with geometry shown in Fig. 1(d). The length of the middle section is still 15 cm.

length of the middle section, which effect is known as the Hartman effect [6] and has been clearly explained elsewhere [7].

The previous section discusses about the modal effect when discontinuities are encountered. However, the modal effect is not necessary in the uniform waveguide. In other words, there is no excitation of high-order modes in that kind of system. For a dielectric loaded waveguide, the measured transmission and group delay agree perfectly with the one-dimensional theory, as expected [14, 15].

4. MULTIPLE RELFECTIONS WITH MODAL EFFECT: ALTERNATIVE EXPLANATION

Since high-order modes are evanescent waves, they decay quickly. The existence of HOMs modifies the amplitude and phase of the transmission and reflection coefficients of the fundamental mode. Multiple reflections are constructed based on two discontinuities, as shown in Fig. 5(a) and Fig. 5(b). Modal analysis is considered, but only the components of the fundamental mode are extracted. The reflection and transmission coefficients of the fundamental TE_{10} mode at the two discontinuities are,

$$\begin{cases} A_1 = |A_1|\, e^{i\phi_a} \\ B_1 = |B_1|\, e^{i\phi_b} \end{cases} \quad \text{and} \quad \begin{cases} A_1' = |A_1'|\, e^{i\phi_a'} \\ B_1' = |B_1'|\, e^{i\phi_b'} \end{cases} \tag{5}$$

These two single-step systems can be used to constitute a potential well (Fig. 1(a)) or a potential barrier (Fig. 1(b)). The complex transmission and reflection coefficients contain the effect of the excitation of higher-order modes. The frequency responses of these two sets of coefficients are depicted in Fig. 5(c) and Fig. 5(d).
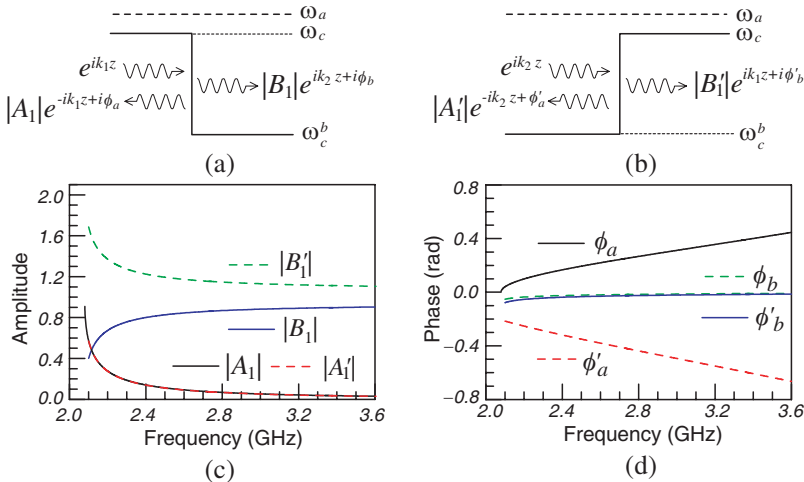
The amplitude of the reflection coefficients (A_1 and A_1') are almost the same, as expected, but B_1 and B_1' differ in amplitude and phase because of the different characteristic impedances of the two sides of a single step.

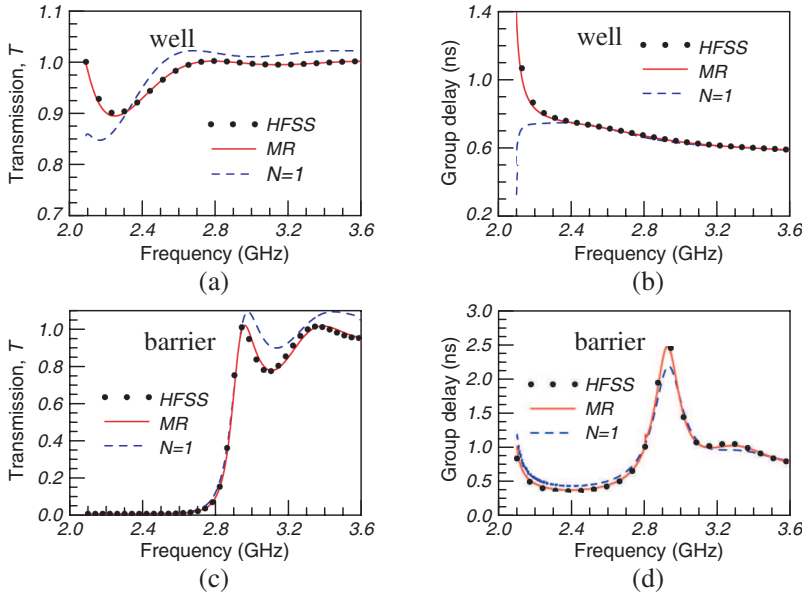When multiple reflections are considered, the transmission coefficient is,

$$
\begin{aligned}
D_1 &= |B_1| \, |B_1'| \, e^{ik_1^c L} e^{i\left(\phi_b + \phi_b'\right)} \sum_{n=0}^{\infty} \left(|A_1'|^2 \right)^n e^{2ni\left(k_1^c L + \phi_a'\right)} \\
&= \frac{|B_1| \, |B_1'| \, e^{ik_1^c L} e^{i\left(\phi_b + \phi_b'\right)}}{1 - |A_1'|^2 \, e^{2i\left(k_1^c L + \phi_a'\right)}}
\end{aligned}
\tag{6}
$$

The format of the transmission coefficient is very similar to that in the single mode case. In this case, however, the modal effect is considered. Fig. 6(a) and Fig. 6(b) present the frequency responses of the transmission and the group delay in the case of the potential well. Ten modes are taken into consideration in the calculation. The calculated results match the simulated ones from HFSS. Fig. 6(c) and Fig. 6(d) plot the results for the potential barrier. Again, the results from the multiple-reflections mechanism are consistent with the results obtained using HFSS.

Although the multiple reflections are constructed with two single-

Figure 5. Schematic diagrams of the single discontinuity (a) from high cutoff to low cutoff, and (b) from low cutoff to high cutoff, (c) amplitudes and (d) phases of the coefficients for the propagating TE_{10} mode when ten high-order modes are considered.

Figure 6. Transmission and group delay for the potential well (a) and (b), and the potential barrier (c) and (d). Solid lines represent the results of multiple-reflection method; dashed lines are the single-mode case; and solid dots are the results obtained using HFSS.

step discontinuities, the results are strongly consistent with the full modal analysis as shown in Fig. 6. The properties of a wave packet can be adjusted by the extra phase which is originated from the effect of high-order evanescent modes. By controlling the extra phase, an apparent superluminal group delay or ultra slow wave can be achieved.

5. CONCLUSION

Modal analysis is conducted to analyze the effect of evanescent modes on the frequency/time domain characteristics of a wave. In the cases of the waveguide discontinuity, the calculated results agree very well with those obtained from HFSS when high-order evanescent modes are considered to satisfy the three-dimensional boundary conditions. The oversized/undersized waveguide is easy to fabricate and can be employed to model its counterpart in quantum mechanics, provided the effects of evanescent modes are considered. Furthermore, controlling the excitation of evanescent modes can manipulate the tunneling characteristics. It is important for numerous applications.

The modal effect is demonstrated to be important. It suggests the necessity to apply the modal analysis to other systems as quantum mechanical system with the geometric discontinuities. The presented theory, however, is based on the frequency domain. To obtain the group delay of a single wave packet, time-domain analysis must be performed, and this part of research is currently under theoretical and experimental investigation. Time-domain analysis may slightly modify the results, but the conclusions are nevertheless valid: high-order modes should be considered. Such an approach is important not only for electromagnetic systems, but also for other tunneling systems with geometric discontinuities.

ACKNOWLEDGMENT

APPENDIX A.

The following modal analysis is applied to analyze a structure consisting of three rectangular waveguides with an oversized or undersized waveguide in the middle, as displayed in Fig. 1(a) or Fig. 1(b). The electric and magnetic fields in the three regions, defined in Fig. 2(b), are as follows.

$$
\text{Region I}
\begin{cases}
E_{y\mathrm{I}} = \sin\left(\dfrac{\pi x}{a}\right)e^{ik_1^a z} + \displaystyle\sum_{n=1}^{\infty} A_n \sin\left(\dfrac{n\pi x}{a}\right)e^{-ik_n^a z} \\[4mm]
H_{x\mathrm{I}} = -\dfrac{1}{Z_1^a}\sin\left(\dfrac{\pi x}{a}\right)e^{ik_1^a z} + \displaystyle\sum_{n=1}^{\infty} \dfrac{1}{Z_n^a} A_n \sin\left(\dfrac{n\pi x}{a}\right)e^{-ik_n^a z}
\end{cases}
\tag{A1}
$$

where $k_n^a = \sqrt{\left(\omega^2 - \omega_{c,na}^2\right)}\Big/ c$ and $Z_n^a = \omega\eta_0/k_n^a c$. k_n^a, Z_n^a, and $\omega_{c,na}$ are the propagation constant, the characteristic impedance, and the cutoff frequency of the nth mode with the waveguide broadside of a, respectively. The other parameters, ω, η_0, and c, are frequency, the characteristic impedance of free space, and the speed of light in vacuum, respectively. A_n is the complex coefficient of the reflected wave of the nth mode. Notably, (A1) is identical to (2). The first term ($n = 1$) in the summation of (A1) is singled out in (2) to express that this term is the only propagation wave (the propagation constant k_1

is real), and the others ($n \geq 2$) are evanescent waves (the propagation constant $k_n = i\kappa_n$ which is pure imaginary).

The field components in region II are,

$$
\text{Region II}
\begin{cases}
E_{y\text{II}} = \displaystyle\sum_{n=1}^{\infty} B_n \sin\left(\frac{n\pi x'}{b}\right) e^{ik_n^b z} + \sum_{n=1}^{\infty} C_n \sin\left(\frac{n\pi x'}{b}\right) e^{-ik_n^b z} \\[3mm]
H_{x\text{II}} = -\displaystyle\sum_{n=1}^{\infty} \frac{1}{Z_n^b} B_n \sin\left(\frac{n\pi x'}{b}\right) e^{ik_n^b z} \\[3mm]
\qquad\quad + \displaystyle\sum_{n=1}^{\infty} \frac{1}{Z_n^b} C_n \sin\left(\frac{n\pi x'}{b}\right) e^{-ik_n^b z}
\end{cases}
\tag{A2}
$$

where k_n^b, Z_n^b, and $\omega_{c,nb}$ are the propagation constant, characteristic impedance, and cutoff frequency of the nth mode with a broadside of b, respectively. B_n is the forward wave coefficient of the nth mode, and C_n, likewise, is the coefficient of nth mode of backward wave which $x' \equiv x - (a-b)/2$. The field components in region III are:

$$
\text{Region III}
\begin{cases}
E_{y\text{III}} = \displaystyle\sum_{n=1}^{\infty} D_n \sin\left(\frac{n\pi x}{a}\right) e^{ik_n^a z} \\[3mm]
H_{x\text{III}} = -\displaystyle\sum_{n=1}^{\infty} \frac{1}{Z_n^a} D_n \sin\left(\frac{n\pi x}{a}\right) e^{ik_n^a z}
\end{cases}
\tag{A3}
$$

where D_n is the transmitted coefficient of the nth mode

Unlike the boundary conditions of quantum mechanics where the wave function and its first derivative are continuous, in electrodynamics, the electric and magnetic field must be continuous. The four boundary conditions in the range $0 \leq x \leq a$ are,

(I) Tangential electric field is continuous at $z = 0$, $E_{y\text{I}}\big|_{z=0} = E_{y\text{II}}\big|_{z=0}$

$$
\sum_{n=1}^{\infty} B_n \sin\left(\frac{n\pi x'}{b}\right) + \sum_{n=1}^{\infty} C_n \sin\left(\frac{n\pi x'}{b}\right)
$$

$$
= \sin\left(\frac{\pi x}{a}\right) + \sum_{n=1}^{\infty} A_n \sin\left(\frac{n\pi x}{a}\right)
\tag{A4a}
$$

(II) Tangential magnetic field is continuous at $z = 0$, $H_{x\text{I}}\big|_{z=0} = H_{x\text{II}}\big|_{z=0}$

$$
\sum_{n=1}^{\infty} k_n^b B_n \sin\left(\frac{n\pi x'}{b}\right) - \sum_{n=1}^{\infty} k_n^b C_n \sin\left(\frac{n\pi x'}{b}\right)
$$

$$
= k_1^a \sin\left(\frac{\pi x}{a}\right) - \sum_{n=1}^{\infty} k_n^a A_n \sin\left(\frac{n\pi x}{a}\right)
\tag{A4b}
$$

(III) Tangential electric field is continuous at $z = L$, $E_{y\mathrm{II}}\,|_{z=L} = E_{y\mathrm{III}}\,|_{z=L}$

$$\sum_{n=1}^{\infty} B_n \sin\left(\frac{n\pi x'}{b}\right) e^{ik_n^b L} + \sum_{n=1}^{\infty} C_n \sin\left(\frac{n\pi x'}{b}\right) e^{-ik_n^b L}$$

$$= \sum_{n=1}^{\infty} D_n \sin\left(\frac{n\pi x}{a}\right) e^{ik_n^a L} \tag{A4c}$$

(IV) Tangential magnetic field is continuous at $z = L$, $H_{x\mathrm{II}}\,|_{z=L} = H_{x\mathrm{III}}\,|_{z=L}$

$$\sum_{n=1}^{\infty} k_n^b B_n \sin\left(\frac{n\pi x'}{b}\right) e^{ik_n^b L} - \sum_{n=1}^{\infty} k_n^b C_n \sin\left(\frac{n\pi x'}{b}\right) e^{-ik_n^b L}$$

$$= \sum_{n=1}^{\infty} k_n^a D_n \sin\left(\frac{n\pi x}{a}\right) e^{ik_n^a L} \tag{A4d}$$

Note here,

$$\begin{cases} E_{y\mathrm{I}}\,|_{z=0} = E_{y\mathrm{III}}\,|_{z=L} = 0 \\ H_{x\mathrm{I}}\,|_{z=0} = H_{x\mathrm{III}}\,|_{z=L} = 0 \end{cases} \quad \text{for} \quad \begin{cases} (a-b)/2 \le x \le 0 \\ a \le x \le (a+b)/2 \end{cases} \tag{A5}$$

Actually, (A4a) to (A4d) and (A5) are the three-dimensional boundary conditions. The three-dimensional electric fields and magnetic fields ($\vec{E}(x,z)$ and $\vec{H}(x,z)$) containing the fundamental mode and some high-order modes are employed to satisfy those conditions. Consequently, this method is called modal analysis which is important for three-dimensional geometrically discontinuous systems.

To calculate the transmission and group delay, we have to solve the coefficient D_n, unlike most literature solving A_n only. Orthogonality and trigonometric identities yields,

$$\begin{cases} \int_0^a \sin\left(\frac{m\pi x}{a}\right) \sin\left(\frac{n\pi x}{a}\right) dx = \frac{a}{2}\delta_{mn} \\ \int_0^b \sin\left(\frac{m\pi x'}{b}\right) \sin\left(\frac{n\pi x'}{b}\right) dx' = \frac{b}{2}\delta_{mn} \end{cases} \tag{A6}$$

and

$$\int_0^b \sin\left(\frac{n\pi x}{a}\right) \sin\left(\frac{m\pi x'}{b}\right) dx' = \int_0^a \sin\left(\frac{n\pi x}{a}\right) \sin\left(\frac{m\pi x'}{b}\right) dx$$

$$\equiv I_{mn}^{ba} = I_{nm}^{ab} \tag{A7}$$

First, multiplying (A4a) by $\sin(m\pi x/a)$ and integrating x from 0 to a, gives,

$$\frac{a}{2}\delta_{m1} + \frac{a}{2}A_m = \sum_{n=1}^{\infty} B_n I_{nm}^{ba} + \sum_{n=1}^{\infty} C_n I_{nm}^{ba} \tag{A8a}$$

Then, multiplying (A4b), (A4c), and (A4d) by $\sin(m\pi x'/b)$ and integrating x' from 0 to b, yields,

$$k_1^a I_{1m}^{ab} - \sum_{n=1}^{\infty} A_n k_n^a I_{nm}^{ab} = \frac{b}{2} k_m^b B_m - \frac{b}{2} k_m^b C_m \tag{A8b}$$

$$\frac{b}{2} B_m e^{ik_m^b L} + \frac{b}{2} C_m e^{-ik_m^b L} = \sum_{n=1}^{\infty} I_{nm}^{ab} D_n e^{ik_n^a L} \tag{A8c}$$

$$\frac{b}{2} B_m k_m^b e^{ik_m^b L} - \frac{b}{2} C_m k_m^b e^{-ik_m^b L} = \sum_{n=1}^{\infty} I_{nm}^{ab} D_n k_n^a e^{ik_n^a L} \tag{A8d}$$

Proper manipulation of (A8c) and (A8d) gives,

$$\begin{cases} B_m = \dfrac{1}{b} e^{-ik_m^b L} \displaystyle\sum_{n=1}^{\infty} I_{nm}^{ab} \left(1 + \dfrac{k_n^a}{k_m^b}\right) D_n e^{ik_n^a L} \\[3mm] C_m = \dfrac{1}{b} e^{ik_m^b L} \displaystyle\sum_{n=1}^{\infty} I_{nm}^{ab} \left(1 - \dfrac{k_n^a}{k_m^b}\right) D_n e^{ik_n^a L} \end{cases} \tag{A9}$$

Substituting B_n and C_n into (A8a) and (A8b) and eliminating A_n yields,

$$ak_1^a I_{1m}^{ab}$$

$$= \sum_{n=1}^{\infty} \left\{ \begin{array}{l} \dfrac{2}{c} \displaystyle\sum_{p=1}^{\infty}\sum_{q=1}^{\infty} k_q^a I_{np}^{ab} I_{pq}^{ba} I_{qm}^{ab} \left[\cos\left(k_p^b L\right) - i\dfrac{k_n^a}{k_p^b}\sin\left(k_p^b L\right)\right] \\[4mm] + \dfrac{a}{2} k_m^b I_{nm}^{ab} \left[-i\sin\left(k_m^b L\right) + \dfrac{k_n^a}{k_m^b}\cos\left(k_m^b L\right)\right] \end{array} \right\} D_n\, e^{ik_n^a L} \tag{A10}$$

In consideration of the first N modes, (A10) can be rewritten as:

$$P_m = \sum_{n=1}^{N} Q_{mn} D_n \tag{A11}$$

where $P_m = ak_1^a I_{1m}^{ab}$ and

$$Q_{mn} = \left\{ \begin{array}{l} \dfrac{2}{b} \displaystyle\sum_{p=1}^{N}\sum_{q=1}^{N} k_q^a I_{np}^{ab} I_{pq}^{ba} I_{qm}^{ab} \left[\cos\left(k_p^b L\right) - i\dfrac{k_n^a}{k_p^b}\sin\left(k_p^b L\right)\right] \\[4mm] + \dfrac{a}{2} k_m^c I_{nm}^{ab} \left[-i\sin\left(k_m^b L\right) + \dfrac{k_n^a}{k_m^b}\cos\left(k_m^b L\right)\right] \end{array} \right\} e^{ik_n^a L}$$

REFERENCES

1. Landauer, R. and T. Martin, "Barrier interaction time in tunneling," *Rev. Mod. Phys.*, Vol. 66, No. 1, 217–228, 1994.

2. Hauge, E. H. and J. A. Stovneng, "Tunneling time: A critical review," *Rev. Mod. Phys.*, Vol. 61, No. 4, 917–936, 1989.

3. Solli, D., R. Y. Chiao, and J. M. Hickmann, "Superluminal effects and negative group delays in electronics, and their applications," *Phys. Rev. E*, Vol. 66, 056601, 2002.

4. Jackson, A. D., A. Lande, and B. Lautrup, "Apparent superluminal behavior in wave propagation," *Phys. Rev. A*, Vol. 64, 044101, 2001.

5. Winful, H. G., "Nature of superluminal barrier tunneling," *Phys. Rev. Lett.*, Vol. 90, 023901, 2003.

6. Hartman, T. E., "Tunneling of a wave packet," *J. Appl. Phys.*, Vol. 33, No. 12, 3427–3433, 1962.

7. Winful, H. G., "Delay time and the hartman effect in quantum tunneling," *Phys. Rev. Lett.*, Vol. 91, 260401, 2003.

8. Stenner, M. D., D. J. Gauthier, and M. A. Neifeld, "Fast causal information transmission in a medium with a slow group velocity," *Phys. Rev. Lett.*, Vol. 94, 053902, 2005.

9. Wang, L. J., A. Kuzmich, and A. Dogariu, "Gain-assisted superluminal light propagation," *Nature*, Vol. 406, 277–279, 2000.

10. Cui, C. L., J. K. Jia, J. W. Gao, Y. Xue, G. Wang, and J. H. Wu, "Ultraslow and superluminal light propagation in a four-level atomic system," *Phys. Rev. A*, Vol. 76, 033815, 2007.

11. Halvorsen, T. G. and J. M. Leinaas, "Superluminal group velocity in a birefringent crystal," *Phys. Rev. A*, Vol. 77 023808, 2008.

12. Steinberg, A. M., P. G. Kwiat, and R. Y. Chiao, "Measurement of the single-photon tunneling time," *Phys. Rev. Lett.*, Vol. 71, No. 5, 708–711, 1993.

13. Von Freymann, G., S. John, S. Wong, V. Kitaev, and G. A. Ozin, "Measurement of group velocity dispersion for finite size three-dimensional photonic crystals in the near-infrared spectral region," *Appl. Phys. Lett.*, Vol. 86, 053108, 2005.

14. Vetter, R. M., A. Haibel, and G. Nimtz, "Negative phase time for scattering at quantum wells: A microwave analogy experiment," *Phys. Rev. E*, Vol. 63, 046701, 2001.

15. Brodowsky, H. M., W. Heitmann, and G. Nimtz, "Comparison of experimental microwave tunneling data with calculations based on Maxwell's equations," *Phys. Lett. A*, Vol. 222, 125–129, 1996.

16. Winful, H. G., "Group delay, stored energy, and the tunneling of evanescent electromagnetic waves," *Phys. Rev. E*, Vol. 68, 016615, 2003.

17. Wang, Z. Y. and C. D. Xiong, "Theoretical evidence for the superluminality of evanescent modes," *Phys. Rev. A*, Vol. 75, 042105, 2007.

18. Chen, X. and C. Xiong, "Electromagnetic simulation of the evanescent mode," *Ann. Phys. (Leipzig)*, Vol. 7, 631, 1998.

19. Pablo, A., L. Barbero, H. E. Hernández-Figueroa, and E. Recami, "Propagation speed of evanescent modes," *Phys. Rev. E*, Vol. 62, No. 6, 8628–8635, 2000.

20. Enders, A. and G. Nimtz, "Photonic-tunneling experiments," *Phys. Rev. B*, Vol. 47, No. 15, 9605–9609, 1993.

21. Enders, A. and G. Nimtz, "Evanescent-mode propagation and quantum tunneling," *Phys. Rev. E*, Vol. 48, No. 1, 632–634, 1993.

22. Winful, H. G., "The meaning of group delay in barrier tunnelling: A re-examination of superluminal group velocities," *New J. Phys.*, Vol. 8, 101, 2006.

23. Fleming, J. G., S. Y. Lin, I. El-Kady, R. Biswas, and K. M. Ho, "All-metallic three-dimensional photonic crystals with a large infrared bandgap," *Nature*, Vol. 417, 52–55, 2002.

24. Capmany, J. and D. Novak, "Microwave photonics combines two worlds," *Nature Photonic*, Vol. 1, 319–330, 2007.

25. Pozar, D. M., *Microwave Engineering*, Chap. 5, Addison-Welsey, New York, 1990.

26. Gesell, G. A. and I. R. Ciric, "Recurrence modal analysis for multiple waveguide discontinuities and its application to circular structures," *IEEE Trans. Microwave Theory Tech.*, Vol. 41, No. 3, 484–490, 1993.

27. Rozzi, T. E. and W. F. G. Mecklenbrauker, "Wide-band network modeling of interacting inductive irises and steps," *IEEE Trans. Microwave Theory Tech.*, Vol. 23, No. 2, 235–24, 1975.

28. Davies, P. C. W., "Quantum tunneling time," *Am. J. Phys.*, Vol. 73, No. 1, 23–27, 2004.